Dexamethasone Stiffens Trabecular Meshwork, Trabecular Meshwork Cells, and Matrix

Vijay Krishna Raghunathan,[1] Joshua T. Morgan,[1] Shin Ae Park,[1] Darren Weber,[2] Brett S. Phinney,[2] Christopher J. Murphy,[1,3] and Paul Russell[1]

[1]Department of Surgical and Radiological Sciences, School of Veterinary Medicine, University of California Davis, Davis, California, United States
[2]University of California Davis Genome Center Proteomics Core Facility, University of California Davis, Davis, California, United States
[3]Department of Ophthalmology and Vision Sciences, School of Medicine, University of California Davis, Davis, California, United States

Correspondence: Paul Russell, Department of Surgical and Radiological Sciences, School of Veterinary Medicine, University of California Davis, Davis, CA 95616, USA; prussell@ucdavis.edu.

VKR and JTM contributed equally to the work presented here and should therefore be regarded as equivalent first authors.

Submitted: February 23, 2015
Accepted: May 22, 2015

Citation: Raghunathan VK, Morgan JT, Park SA, et al. Dexamethasone stiffens trabecular meshwork, trabecular meshwork cells, and matrix. *Invest Ophthalmol Vis Sci*. 2015;56:4447–4459. DOI:10.1167/iovs.15-16739

Purpose. Treatment with corticosteroids can result in ocular hypertension and may lead to the development of steroid-induced glaucoma. The extent to which biomechanical changes in trabecular meshwork (TM) cells and extracellular matrix (ECM) contribute toward this dysfunction is poorly understood.

Methods. Primary human TM (HTM) cells were cultured for either 3 days or 4 weeks in the presence or absence of dexamethasone (DEX), and cell mechanics, matrix mechanics and proteomics were determined, respectively. Adult rabbits were treated topically with either 0.1% DEX or vehicle over 3 weeks, and mechanics of the TM were determined.

Results. Treatment with DEX for 3 days resulted in a 2-fold increase in HTM cell stiffness, and this correlated with activation of extracellular signal-related kinase 1/2 (ERK1/2) and overexpression of α-smooth muscle actin (αSMA). Further, the matrix deposited by HTM cells chronically treated with DEX is approximately 4-fold stiffer, more organized, and has elevated expression of matrix proteins commonly implicated in glaucoma (decorin, myocilin, fibrillin, secreted frizzle-related protein [SFRP1], matrix-gla). Also, DEX treatment resulted in a 3.5-fold increase in stiffness of the rabbit TM.

Discussion. This integrated approach clearly demonstrates that DEX treatment increases TM cell stiffness concurrent with elevated αSMA expression and activation of the mitogen-activated protein kinase (MAPK) pathway, stiffens the ECM in vitro along with upregulation of Wnt antagonists and fibrotic markers embedded in a more organized matrix, and increases the stiffness of TM tissues in vivo. These results demonstrate glucocorticoid treatment can initiate the biophysical alteration associated with increased resistance to aqueous humor outflow and the resultant increase in IOP.

Keywords: cell and matrix mechanics, steroid-induced glaucoma, extracellular matrix, elastic modulus, proteomics

Glaucoma is a group of diseases, affecting over 60 million people worldwide, defined by irreversible damage to the optic nerve leading to vision loss and blindness.[1] In primary open angle glaucoma (POAG), resistance to aqueous humor outflow by the trabecular meshwork (TM) leads to elevated IOP. Intraocular pressure remains the only modifiable, causative risk factor for glaucoma progression. Therefore, understanding pathological changes to the TM is of central importance to developing effective therapeutics. Alterations in tissue biomechanics are an underexplored component of this pathology. We recently demonstrated that the glaucomatous TM is approximately 20-fold stiffer than normal,[2] and it is unclear whether this increase in stiffness is a result of changes to extracellular matrix (ECM) stiffness and/or cell stiffness. There is circumstantial evidence to support mechanical changes in cellular and extracellular constituents of the TM. Primary open-angle glaucoma has been associated with altered TM cell cytoskeletal dynamics[3,4] as well as significant changes to the composition and morphology of the TM.[5] The underlying mechanisms for dysregulation of TM cytoskeletal dynamics, and ECM deposition and remodeling remain poorly understood. It is possible that cytoskeletal changes are secondary to ECM alterations through integrin signaling.[6,7] While not directly linked to stiffening in the TM, cells/tissues of POAG patients exhibit elevated levels of transglutaminase (TGM2, a crosslinker of ECM proteins) and alkaline phosphatase (ALP, a calcification marker), both associated with stiffening of the ECM in other systems.[8–12] In aggregate, these findings point toward cellular and ECM contributions to the observed stiffening of the human TM (HTM) in POAG. Despite the known importance of biophysical cues to TM cell function,[13–17] biophysical signaling within the TM remains poorly understood.

Studying the biophysical properties of the TM is inherently challenging due to the lack of suitable in vivo models. Primary open-angle glaucoma is in general a human disease, since the manifestation of glaucoma in other species does not exhibit many of the features found in human POAG patients. As such, in vitro culture of HTM cells is commonly used to investigate alterations in molecular signaling as well as biomechanical properties. One of the most commonly used in vitro models

involves the use of glucocorticoids (GCs), a family of steroid hormones that bind to the GC receptor.[18] These compounds have been associated with glaucoma, since patients with POAG have increased cortisol levels,[19,20] although responses to cortisol may vary between individuals.[21–24] Approximately 30% to 40% of the normotensive population develops elevated IOP when treated with ocular GCs, such as dexamethasone (DEX). This increase in IOP is a recognized risk factor associated with glaucoma, and necessitates cessation of steroid use and/or therapeutic intervention in these individuals.[25] Additionally, almost all POAG patients respond to steroids by developing a significantly higher IOP.[25–27] The mechanisms of steroid-induced ocular hypertension currently are not understood. However, in line with our finding of increased stiffness in POAG, we hypothesize that DEX induces stiffening of TM tissue. Further, considering findings that DEX alters TM cell actin cytoskeletal dynamics,[4] cellular proteomic profile,[28] and ECM production,[29–31] we hypothesize that DEX induces intrinsic stiffening of TM cells as well as the elaboration of a stiffer matrix.

To test our hypothesis, we measured the biomechanical properties of HTM cells and their ECM as well as determining the alterations in the proteins present in the ECM after DEX treatment. To establish the relevance of our in vitro findings, we topically administered DEX to rabbit eyes for 3 weeks and examined changes to the stiffness of the meshwork in vivo.

Materials and Methods

Isolation and Culture of HTM Cells

Primary HTM cells were isolated from donor corneoscleral rims unsuitable for transplant (SavingSight Eye Bank, St. Louis, MO, USA) as described previously.[32] Since cells were obtained from donor tissue, these are not considered as Human Subject Research. All experiments involving human tissue/cells were performed in compliance with the tenets of the Declaration of Helsinki. Power analyses ($\alpha = 0.05$) indicated that three donor cell lines would be necessary when differences of the means of elastic modulus (our primary end-point for tissue mechanics) are small (0.5 kPa) and the standard deviations are large (0.1 kPa). We used HTM cells isolated from at least three or four donors for each experiment and they were routinely maintained in Dulbecco's modified Eagle medium/Nutrient Mixture F-12 (50:50; DMEM/F-12) supplemented with 10% fetal bovine serum (FBS), and 1% penicillin/streptomycin/amphotericin (Life Technologies, Carlsbad, CA, USA). Cells were used between passages three and seven for all experiments. All cultures were confirmed as HTM by myocilin gene upregulation in response to 100 nM DEX (Sigma-Aldrich Corp., St. Louis, MO, USA). Equivolume treatments of ethanol (EtOH) were used as the vehicle control.

Treatment With DEX

Cell Mechanics. To determine changes in cellular mechanics, cells were seeded on glass coverslips (50,000/well) in a 24-well plate and allowed to attach overnight. Media was changed the following day with vehicle control (EtOH) or 100 nM DEX and incubated for 3 days. Coverslips then were mounted on atomic force microscope (AFM) compatible petri dishes and equilibrated for 30 min in Hank's balanced salt solution (HBSS) immediately before obtaining force versus indentation curves.

ECM Mechanics. For these experiments, cells were cultured on amino-silane modified glass coverslips. Briefly, glass coverslips were incubated with 3-aminopropyl trimethoxysilane overnight under vacuum. Silanized coverlips were heat treated at 200°C for 20 minutes and stored briefly under vacuum with a desiccant until used for cell culture. Freshly silanized coverslips were used for all experiments. Primary HTM cells were seeded on these modified coverslips (50,000/well) in 24-well dishes as described above. Dexamethasone or EtOH treatment was performed twice every week for 4 weeks.

Isolation of Protein and Western Blotting

Changes in cell stiffness were correlated with alterations in protein expression by Western blotting. Briefly, following 3-day DEX treatments, cells were lysed and scraped into radioimmunoprecipitation assay (RIPA) buffer (ThermoScientific, Waltham, MA, USA) supplemented with protease and phosphatase inhibitors (Fisher Scientific, Hampton, NH, USA) on ice. The cells then were homogenized and centrifuged at 1000*g* for 1 minute to remove any cell debris. Homogenate was concentrated using 3000 Dalton cut-off spin columns (Fisher Scientific). Protein was quantified using a modified Lowry assay (DC assay; BioRad, Hercules, CA, USA) with BSA as the standard. Protein homogenate then was denatured in Laemmli buffer (Sigma-Aldrich Corp.) by boiling for 10 minutes. Approximately 10 μg protein was loaded per well for each sample. Electrophoresis was performed using 10% Bis-Tris precast gels as described previously[13] and protein was transferred onto nitrocellulose membranes. Immunoblotting was done against anti–α-smooth muscle actin (αSMA; Sigma-Aldrich Corp.), total extracellular signal-regulated kinase 1/2 (ERK1/2; Abcam, Cambridge, MA, USA), phosphorylated ERK1/2 (pERK1/2; Abcam), and β-tubulin (Abcam) overnight at 4°C. This was followed by incubation with secondary antibodies conjugated with horseradish peroxidase (HRP; Kirkegaard & Perry Laboratories, Inc., MD, USA) for 1 hour at 37°C. Protein bands were detected by chemiluminescence (Advansta, Inc., Menlo Park, CA, USA). Blots then were imaged using ImageQuant 350 imaging system (GE Healthcare Life Sciences, Pittsburgh, PA, USA). The optical densities of the protein bands were quantified using ImageJ (National Institutes of Health [NIH], Bethesda, MD, USA).[33,34] The staining of the β-tubulin was used as a standard on all blots so that relative quantitation could be determined.

Decellularization and Characterization of the ECM

Matrices were obtained by decellularization of cultures as described previously using 20 mM ammonium hydroxide (NH_4OH).[35] Freshly decellularized ECM was used for mechanical characterization and proteomics, while formaldehyde-fixed cell-derived matrices were used for immunocytochemistry. For mechanical characterization, decellularized matrices were rinsed gently yet thoroughly in HBSS, and AFM was performed in contact mode. Subsequently, decellularization was confirmed by immunocytochemistry. For confirmation, the cell-derived matrices were fixed in 4% formaldehyde for 20 minutes and then labeled for pan-collagen (Abcam), fibronectin (Abcam), F-actin (Phalloidin; Life Technologies), and counterstained with 4′6-diamidino-2-phenylindole (DAPI; Life Technologies) for the presence of nuclear material. The samples then were imaged using a Zeiss 200 M inverted epifluorescence microscope (Carl Zeiss, Jena, Germany). Proteomic profiling was conducted on freshly decellularized ECM as described previously using shotgun proteomics.[35] Total spectral counts of all proteins identified can be found as supplementary data (Supplementary Data S1).

Gene Ontology (GO) Analysis. Functional annotation of the differentially expressed proteins were analyzed using the Database for Annotation, Visualization, and Integrated Discovery (DAVID).[36] Only GO clusters whose *P* value was less than 0.05 were considered.

Investigative Ophthalmology & Visual Science

Table. The Important Biological Functions (With Greatest Statistical Significance for Enrichment) as Defined by GO Classification in the Collected Proteome Data Set of ECM From DEX-Treated Cells That Were Altered at Least 1.9-Fold in Comparison With Control Cultures Using DAVID Proteomic Tool

GO:Term ID	Category	Genes	*P* Value
GO:0044421	Extracellular region part	*WNT5A*, *RBP4*, *A2M*, *ADAMTSL1*, *LTBP2*, *LUM*, *IGFBP7*, *TNC*, *CLU*, *POSTN*, *VTN*, *DCN*, *AHSG*, *TGFB2*, *CTGF*, *SMOC1*, *APOH*, *PTN*, *COL12A1*, *FBN2*, *LAMB1*, *COL8A1*, *THBS1*, *TFPI2*, *COL11A1*, *PRSS12*, *MYOC*, *ADAM9*, *ANGPTL4*, *THBS4*, *MATN2*, *ICAM1*, *COL4A1*, *FBN1*, *CCDC80*, *MGP*, *IGF2*, *NID1*, *SOD1*, *DKK2*, *AFP*, *SERPINF1*, *SFRP1*, *SULF1*, *IGFBP2*, *IGFBP3*, *IGFBP5*	3.72E-29
GO:0005576	Extracellular region	*A2M*, *LTBP2*, *IGFBP7*, *VTN*, *POSTN*, *EDIL3*, *TTN*, *TGFB2*, *CTGF*, *ITIH4*, *APOH*, *COL12A1*, *LTF*, *ITIH2*, *COL11A1*, *TFPI2*, *ADAM9*, *CYR61*, *MATN2*, *ICAM1*, *MFI2*, *MGP*, *SERPINF1*, *WNT5A*, *RBP4*, *ADAMTSL1*, *LUM*, *TNC*, *CLU*, *DCN*, *MDK*, *AHSG*, *SMOC1*, *PTN*, *FBN2*, *COL8A1*, *LAMB1*, *THBS1*, *PRSS12*, *MYOC*, *THBS4*, *ANGPTL4*, *COL4A1*, *FBN1*, *CCDC80*, *IGF2*, *NID1*, *SOD1*, *DKK2*, *AFP*, *DKK1*, *SRPX2*, *TFRC*, *SFRP1*, *SULF1*, *IGFBP2*, *IGFBP3*, *IGFBP5*	1.07E-25
GO:0031012	Extracellular matrix	*WNT5A*, *ADAMTSL1*, *LTBP2*, *TNC*, *LUM*, *POSTN*, *VTN*, *DCN*, *TGFB2*, *AHSG*, *CTGF*, *SMOC1*, *COL12A1*, *FBN2*, *LAMB1*, *THBS1*, *COL8A1*, *TFPI2*, *COL11A1*, *PRSS12*, *THBS4*, *ANGPTL4*, *MATN2*, *COL4A1*, *FBN1*, *CCDC80*, *MGP*, *NID1*, *SOD1*	4.46E-23
GO:0005578	Proteinaceous extracellular matrix	*WNT5A*, *MATN2*, *ADAMTSL1*, *COL4A1*, *LTBP2*, *TNC*, *LUM*, *FBN1*, *CCDC80*, *MGP*, *NID1*, *VTN*, *POSTN*, *DCN*, *CTGF*, *SMOC1*, *COL12A1*, *FBN2*, *LAMB1*, *COL8A1*, *TFPI2*, *COL11A1*, *THBS4*, *ANGPTL4*	9.44E-18
GO:0005615	Extracellular space	*WNT5A*, *RBP4*, *A2M*, *IGFBP7*, *CLU*, *VTN*, *TGFB2*, *AHSG*, *APOH*, *PTN*, *THBS1*, *MYOC*, *ADAM9*, *ANGPTL4*, *ICAM1*, *FBN1*, *MGP*, *IGF2*, *SOD1*, *DKK2*, *AFP*, *SFRP1*, *SERPINF1*, *SULF1*, *IGFBP2*, *IGFBP3*, *IGFBP5*	2.63E-13
GO:0044420	Extracellular matrix part	*COL4A1*, *TNC*, *SMOC1*, *LUM*, *FBN1*, *CCDC80*, *COL12A1*, *NID1*, *LAMB1*, *COL8A1*, *COL11A1*, *PRSS12*	3.66E-10
GO:0009986	Cell surface	*ICAM1*, *LRP1*, *ITGA5*, *CRYAB*, *ITGAV*, *SULF1*, *APOH*, *ITGA2*, *THBS1*, *ITGB1*, *ADAM9*, *HSPA9*	2.29E-05
GO:0031410	Cytoplasmic vesicle	*A2M*, *CLU*, *SOD1*, *ITGB1*, *TGFB2*, *LRP1*, *SERPINF1*, *TFRC*, *SDCBP*, *THBS1*, *IGFBP2*, *MYOF*, *PRSS12*, *THBS4*	3.79E-04
GO:0031982	Vesicle	*A2M*, *CLU*, *SOD1*, *ITGB1*, *TGFB2*, *LRP1*, *SERPINF1*, *TFRC*, *SDCBP*, *THBS1*, *IGFBP2*, *MYOF*, *PRSS12*, *THBS4*	5.69E-04
GO:0016023	Cytoplasmic membrane-bounded vesicle	*A2M*, *LRP1*, *TFRC*, *SERPINF1*, *CLU*, *SDCBP*, *THBS1*, *ITGB1*, *THBS4*, *TGFB2*	1.23E-02
GO:0031988	Membrane-bounded vesicle	*A2M*, *LRP1*, *TFRC*, *SERPINF1*, *CLU*, *SDCBP*, *THBS1*, *ITGB1*, *THBS4*, *TGFB2*	1.49E-02
GO:0042995	Cell projection	*LRP1*, *ITGA5*, *ITGA2*, *SOD1*, *ITGB1*, *DBN1*, *PRSS12*, *MYOC*, *CTNNB1*, *TGFB2*, *CTNNA2*	1.97E-02

The enrichment *P* value (compared to the theoretical human proteome) is calculated based on EASE Score, a modified Fisher's exact test and ranges from 0 to 1. Fisher's exact *P* value = 0 represents perfect enrichment.

Kyoto Encyclopedia of Genes and Genomes (KEGG) Analysis. Analyses were done using the differentially expressed proteins whose *P* values were less than 0.05, using the R-package "Gostats" combining two databases: KEGG pathway database and Molecular Signatures Database from Broad Institute. In the pathway graph, the center part of the dot represents the enrichment of upregulated genes and the outer layer of the dot corresponds to the enrichment of the downregulated genes. Red center at the nodes indicates that the protein set is enriched in proteins that are upregulated, gray indicates proteins that are not enriched in the downregulated group. Green edge color indicates that there are overlapped proteins (similarity) between the two nodes connecting the upregulated proteins. Blue edge color indicates that there are overlapped proteins between the two nodes connecting the downregulated proteins. A solid red node means that this gene set is enriched in up- and downregulated genes. The Table lists the proteins that each cluster interacts with.

Determination of Elastic Modulus

Elastic moduli of cells and matrices were determined by atomic force microscopy. Force versus indentation curves were obtained in contact mode using an Asylum MFP-3D BIO microscope (Asylum Research, Santa Barbara, CA, USA) as described previously.[35,37–39]

Imaging the ECM

Immediately after obtaining force measurements on the decellularized ECM samples, they were rinsed thoroughly in deionized water (dH_2O) and air-dried overnight at 37°C. Then, ECM samples were imaged by the atomic force microscope in contact mode using an AC240TS cantilever (nominal $\kappa = 1.5$ N/m; NanoAndMore, Soquel, CA, USA) at 500 pN applied force and 0.3 Hz.

Treatment of Rabbits With DEX and Clinical Follow-Up

Power analyses ($\alpha = 0.05$) indicated that three animals would be necessary when differences of the means of elastic modulus (our primary end-point for tissue mechanics) are small (1 kPa) and the standard deviations are large (0.3 kPa). Therefore, we used four animals to obtain greater statistical power and to minimize animal use. Four healthy female New Zealand white rabbits (Charles River Laboratories, Wilmington, MA, USA), 14 months old, were included in the study. Each rabbit underwent

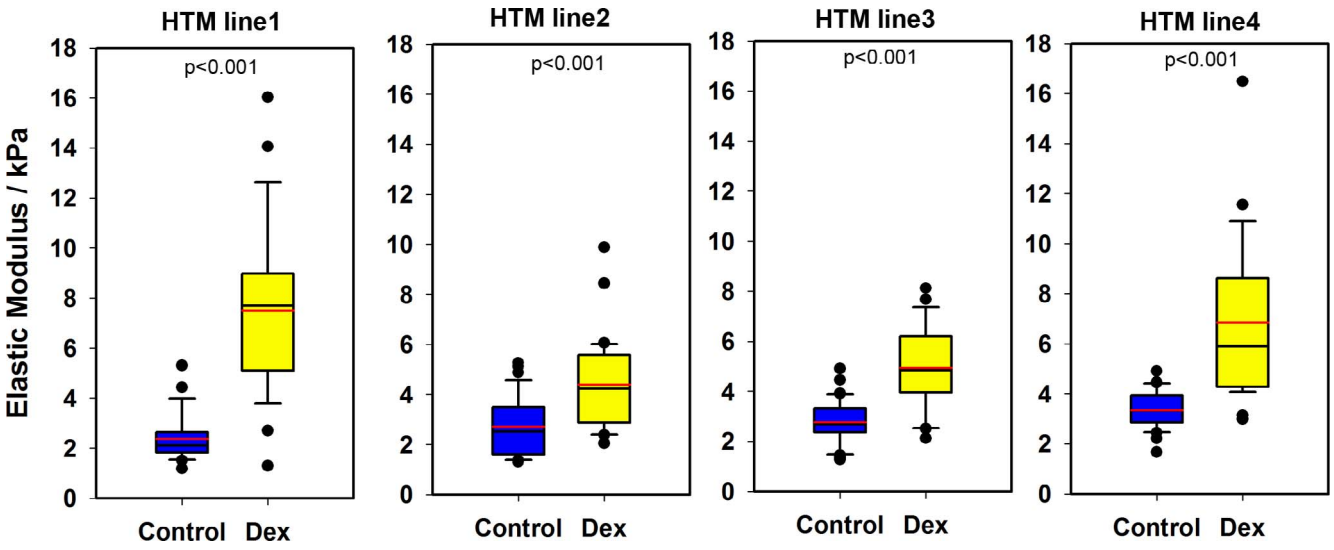

FIGURE 1. Elastic modulus of HTM cells from four donors treated with either vehicle control or DEX for 3 days. Data are represented as *box plots* with mean indicated as a *red line*. Results are from at least seven locations with five force curves per location. $P < 0.001$, Mann-Whitney U test.

a physical examination and was assessed as normal before initiation of the study. A complete ophthalmic examination, including slit-lamp biomicroscopy and indirect ophthalmoscopy, was performed to verify all rabbits had eyes without preexisting ocular diseases. All procedures adhered to the ARVO Statement for the Use of Animals in Ophthalmic and Vision Research, and standards for the care and use of laboratory animals at University of California, Davis, and were approved by the Institutional Animal Care and Use Committee (IACUC). In accordance with the approved IACUC protocol, only one eye could be treated to prevent inadvertent alteration of vision in both eyes and, as such, the contralateral eye was left untreated and was used as the control eye.

Before the initiation of the study, baseline IOPs were measured with a rebound tonometer (Tonovet; Icare, Helsinki, Finland) three times a week for 3 weeks at 9 to 11 AM. At each session, three consecutive measurements were performed by one examiner following 30 minutes of acclimation inside the carrier placed in the examination room, and then 3 to 5 minutes of acclimation on the table to ensure the rabbit was not overstressed, which can result in a temporarily high IOP. Once rigorous baseline data were established, a drop of 0.1% DEX (dexamethasone sodium phosphate; Bausch & Lomb, Tampa, FL, USA) was instilled into the right eye three times daily for 3 weeks. Intraocular pressures were measured daily in the same manner. A complete ophthalmic examination with a slit-lamp biomicroscope and indirect ophthalmoscope was performed five times a week during the study period. The anterior segment was photo-documented using a Nikon SLR digital camera (Nikon, Tokyo, Japan) with macrolens and ring Q2 flash once weekly. The fundus was imaged with a fundus camera (Cf-1 Digital Retinal Camera; Canon, Lake Success, NY, USA) and spectral domain optical coherence tomography (Optovue, Fremont, CA, USA) at the same time points.

Statistical Analysis

All mechanics data are represented as box and whisker plots to demonstrate data distribution. Statistical comparison of mechanics between vehicle and DEX-treated cells was done using Mann-Whitney U test and results are indicated in the plots. Shotgun proteomics data were analyzed using Scaffold Viewer (Proteome Software, Inc., Portland, OR, USA). Using the built-in features of the software, normalized total spectral counts from the five different cell cultures were compared for fold-change between the EtOH and DEX samples. The relative abundance between the two groups was compared using Fisher's exact test.[40] Principal component analysis (PCA) was calculated using the *prcomp* function in R (v 3.1.2; http://www.r-project.org/) on the peptide MS1 spectral count at the protein level using a covariance matrix. The scree plot is plotted as proportion of variance against the number of principal components (PCs).

RESULTS

Alterations to Cell Stiffness and Cytoskeletal Dynamics in HTM Cells In Vitro

The extents to which the biophysical properties of cells and cytoskeletal dynamics are altered with 3-day DEX treatment were evaluated using primary HTM cells. To determine the effect of DEX treatment on cell stiffness, elastic modulus was determined by atomic force microscopy on cells from four individual donors. The distribution of the elastic moduli values for each donor is shown in Figure 1. Three-day DEX treatment induced a significant increase in HTM cell stiffness, from 2.82 ± 1.01 to 5.87 ± 2.93 kPa. Data demonstrated that for all donors, the elastic moduli of DEX-treated cells were significantly greater than those of vehicle (EtOH)–treated cells.

To ascertain if the change in cell stiffness was accompanied by cytoskeletal changes and subsequent activation of the cell's contractility machinery, Western blotting was performed to determine the expression of αSMA and activation of the ERK protein, after DEX treatment (Fig. 2). For all four donor cells, 3-day DEX treatment resulted in significantly elevated expression of αSMA and phosphorylated ERK1/2 with no changes observed for total ERK1/2 or β-tubulin expression. When normalized to the loading control (β-tubulin) expression of αSMA and pERK1/2 in the DEX-treated cells were approximately 2-fold greater than that of vehicle-treated cells.

Human TM cells from three donors also were cultured for 4 weeks in the presence of either vehicle or DEX to allow for deposition of ECM. A subset of samples were fixed and immunostained (F-actin and DAPI) to demonstrate presence of cells after 4 weeks in culture. Consistent with the upregulation of αSMA and pERK1/2 (with 3-day DEX treatment), increased

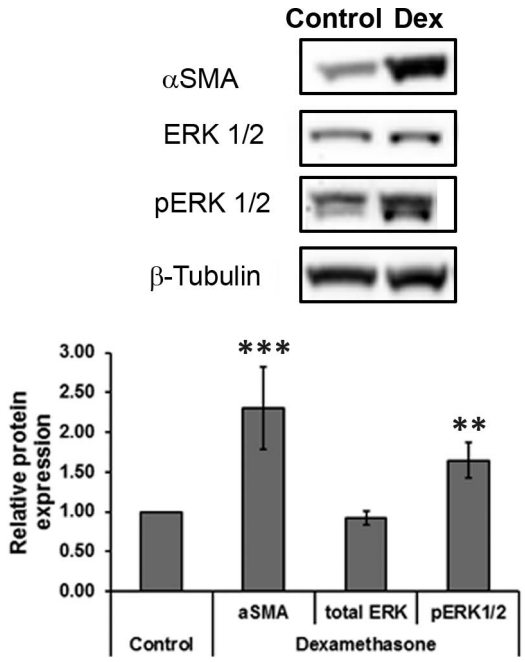

FIGURE 2. Representative Western blot comparing the expressions of αSMA, ERK1/2, phosphorylated ERK1/2, and loading control (β-tubulin) in 3-day control and DEX-treated cells. Graph illustrates the mean optical density of the protein bands expressed relative to control cultures. Data are mean ± SD ($n = 4$ donors). $^{***}P < 0.001$, $^{**}P < 0.01$, Mann-Whitney U test.

numbers of stress fibers were observed in HTM cells treated with DEX (for 4 weeks) compared to control cultures (Fig. 3). Also, consistent with previously established reports, DEX-treated HTM cells appeared enlarged.

Long-Term Effects of DEX Treatment on Matrix Mechanics, Morphology, and Composition In Vitro

Matrix Morphology. To remove the cells while preserving ECM integrity, we lysed the cells using 20 mM NH_4OH and 0.05% Triton X-100 in PBS. Decellularization was confirmed by immunocytochemistry (Fig. 4A). All ECM samples stained positively for pan-collagen with simultaneous lack of F-actin or DAPI staining indicating the ECM was devoid of cytoskeletal or nuclear components after the decellularization. Also, dramatic differences in immunostaining patterns for deposition of fibronectin were observed (Fig. 4A). Fibronectin was observed to be deposited as an organized fibrillar sheet from DEX-treated cells compared to minimal organization observed in the ECM of EtOH-treated cells.

Concurrent with changes in immunostaining, morphological alterations to the deposited ECM were determined by imaging using the AFM. Extracellular matrix deposited by DEX-treated cells appeared more organized and fibrillar in comparison with vehicle-treated cells. As a quantitative measure of matrix roughness, we compared the root mean square (RMS) of the AFM height map of matrix deposited by control cells (216.50 ± 97.75 nm) and DEX-treated cells (85.94 ± 29.09 nm). Quantitative analyses of four random regions of the ECM revealed that DEX treatment resulted in a significantly smoother matrix than controls (Fig. 4B).

Matrix Mechanics. Analysis of force versus indentation curves to determine the elastic moduli of HTM cell–derived ECM revealed that DEX treatment deposited a significantly stiffer ECM compared to EtOH-treated cells (Fig. 5). The elastic moduli for ECM derived from EtOH-treated cells had a mean of 0.37 ± 0.26 kPa, while those derived after DEX treatment had a mean of 1.35 ± 0.45 kPa. The distributions of elastic moduli for each donor cell are illustrated in Figure 5.

Proteomic Analysis of the ECM. To ascertain quantitative differences in biochemical composition of ECM derived from cells chronically treated (for 4 weeks) with EtOH and DEX, nano-scale liquid chromatography tandem-mass spectrometry (nano–LC-MS/MS) was performed on ECM protein extracts. Principal component analysis was performed on the spectral data comparing EtOH- and DEX-derived ECM samples. The Scree plot demonstrated that 97% of the variance in the data was accounted by PCs 1 and 2 (Fig. 6A). Plots of PC1 versus PC2 demonstrated distinct clustering of data (Fig. 6A) suggesting that significant differences in protein expression between the groups existed. Indeed, on closer inspection, it was observed that a significant number of extracellular proteins were up-/downregulated over 1.9-fold after DEX treatment (Fig. 6B; $P < 0.05$, Fisher's exact test). As expected, myocilin (MYOC), a protein known to be upregulated in TM cells by GCs, was significantly upregulated in ECM derived from DEX-treated cells. Detection of MYOC, albeit to a limited extent, was observed in only one of the five donor cell lines in vehicle-treated cell derived matrix. Gene ontology analysis of the expressed proteins is presented in the Table and visualized using the web-based AmiGO2 tool (Supplementary Fig. S1).

Proteins of particular interest that were significantly overexpressed in the ECM derived from DEX-treated cells were Dickkopf-related proteins 1 and 2 (DKK1, DKK2), secreted frizzled-related protein (SFRP1), decorin (DCN), thrombospondin, Wnt5a, extracellular sulfatase 1 (SULF1),

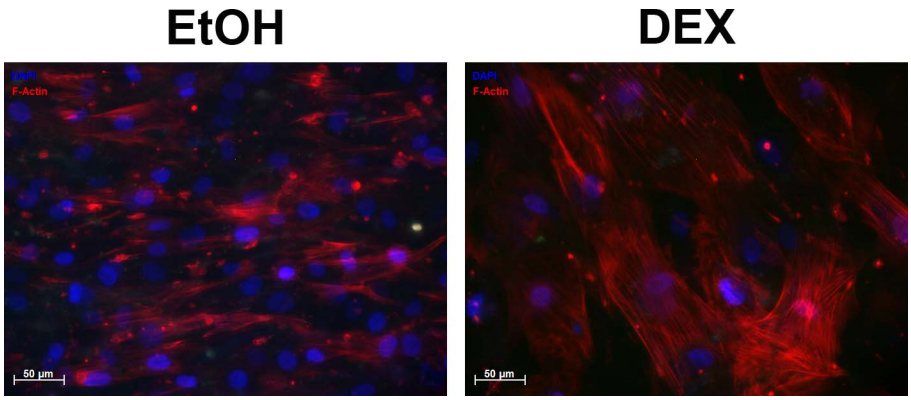

FIGURE 3. Representative images of HTM cells treated with vehicle control or DEX after 4 weeks. Significantly greater number of stress fibers (F-actin/*red*; nucleus/DAPI/*blue*) was observed in the DEX group compared to control (EtOH) cells.

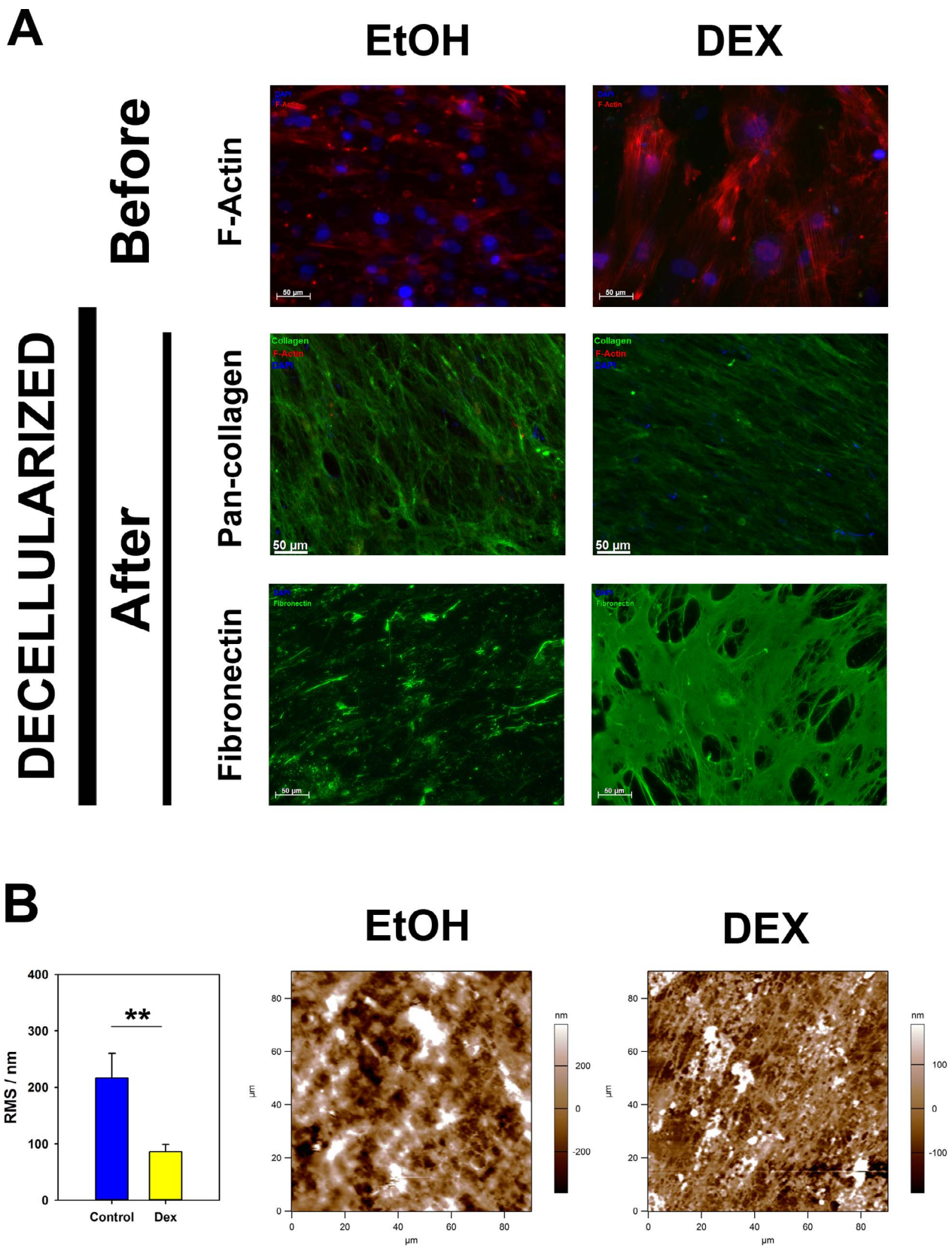

Figure 4. (**A**) Representative images of HTM cell-derived ECM from control or DEX-treated cultures. Absence of staining for F-actin (Phalloidin/*red*) and nuclei (DAPI/*blue*) with abundant signal for pan-collagen immunostaining (*green*) demonstrated the presence of ECM devoid of HTM cells after they were removed with NH_4OH. Differences in assembly and immunostaining pattern for fibronectin were observed between the two groups. *Scale bars*: 50 µm. (**B**) Representative images of ECM morphology as imaged by atomic force microscopy and surface roughness measured as RMS are illustrated. The control ECM was not organized, while the ECM from the DEX-treated cells had a much more organized appearance. Results are mean ± SD of RMS calculated from three images for each donor. $^{**}P < 0.01$, Mann-Whitney *U* test.

Investigative Ophthalmology & Visual Science

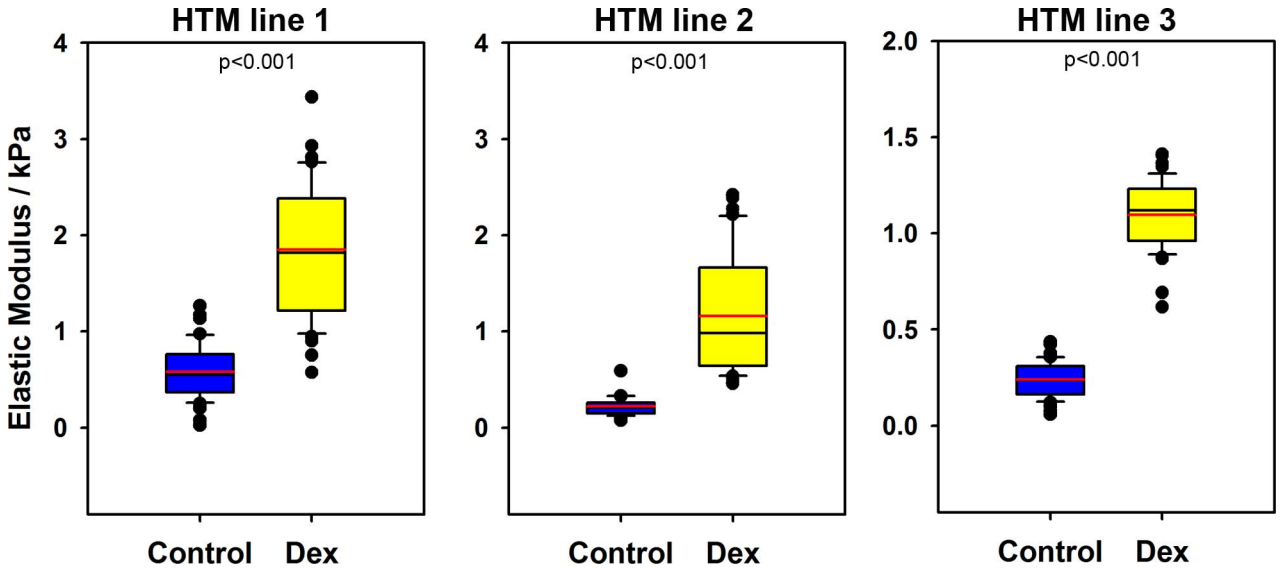

FIGURE 5. Elastic modulus of ECM derived from HTM cells treated with either vehicle control or DEX for 4 weeks. Data are represented as *box plots* with mean indicated as a *red line*. Results are from at least seven locations with five force curves per location. $P < 0.001$, Mann-Whitney U test.

connective tissue growth factor (CTGF), TGF-β2, coiled-coil domain containing protein-80 (CCDC80), lumican, CYR61, vitronectin, and collagens XII and IV. Interestingly, expression of periostin and tenascin-C was dramatically downregulated in ECM derived from DEX-treated cells. Although there was a differential staining pattern of fibronectin by immunocytochemistry, no significant difference in its protein expression in the ECM was observed between EtOH- and DEX-treated samples. Protein–protein interaction analysis using the KEGG pathway was performed on the data obtained by proteomics (Fig. 6C, Supplementary Fig. S2). The most abundantly enriched protein clusters accounted for those that interact with fibronectin, decorin, insulin-like growth factor binding protein 2 (IGFBP2), matrix metalloproteinase 2 (MMP2), focal adhesions, and ECM-receptor interactions. A list of proteins that interact with these clusters and were identified by proteomic analysis of the ECM is provided in Figure 6C.

Effect of DEX on TM Biomechanics In Vivo

Biomechanical characterization of the rabbit TM after topical administration of DEX for 3 weeks was performed by AFM. No ocular toxicity or deleterious health effects were observed in the treated animals during the duration of the study, with the exception of temporary mild conjunctival congestion and chemosis observed in the treated eye of two animals 8 and 9 days after the initiation of the treatment. To facilitate the isolation of an adequately-sized TM sample, we used 14-month-old rabbits. The elastic modulus of the meshwork from all DEX-treated rabbit eyes was significantly higher than the contralateral eyes. The elastic moduli for control rabbit TM had a mean of 1.03 ± 0.55 kPa (mean ± SD), which was significantly increased by DEX treatment to 3.89 ± 2.55 kPa. The distributions of elastic moduli for each rabbit are illustrated in Figure 7A. As expected, between rabbits there were variations in the moduli of the meshworks; but for each rabbit there was an increase in modulus in the DEX-treated eye compared to the contralateral eye. With the four rabbits in our study, no statistically significant changes in IOP were observed between the DEX-treated and control eyes in the 3-week period. We note that the rabbits we investigated were older and this is consistent with previous reports showing induction of an elevated IOP after DEX treatment is blunted in older rabbits.[41,42] As demonstrated by those studies, with increasing age of the rabbit, changes in IOP become smaller and would be expected to be a little less than 1 mm Hg in the older rabbits. Since our rabbits were mature adults, it would have required a substantial number of animals to document statistically significant changes in IOP. The IOP measurements from the rabbits are presented in Figure 7B.

DISCUSSION

While steroids are used widely for the treatment of autoimmune and inflammatory diseases, the development of steroid-induced iatrogenic glaucoma and ocular hypertension is a frequent and potentially debilitating side effect. Pathophysiological investigations of human eyes from patients with steroid-induced glaucoma have correlated the increased resistance to outflow with ultrastructural changes to the TM tissue associated with increased deposition of ECM proteins in the TM beams, deposits in the uveal meshwork and juxtacanalicular (JCT) region.[5,43,44] It also has been speculated that cytoskeletal changes of cells in the Schlemm's canal and JCT may contribute to the onset and progression of the disease. While these changes have been linked to the outflow pathway, biomechanical changes to TM cells, ECM, and tissue have not been reported previously to our knowledge.

DEX Alters Cytoskeletal Dynamics and Cell Stiffness In Vitro

Cytoskeletal remodeling of TM cells after DEX treatment has been demonstrated previously through the formation of polygonal actin networks, noncanonical Wnt signaling, and activation of the Rho family of proteins.[4,45–47] These cross-linked actin structures have been linked to the formation of stress fibers and the induction of contractile machinery of the cell.[7] It is well established that TM contractility is an important regulator of IOP regulation and several therapeutics targeting contractility currently are being developed for clinical applications.[48,49] Interestingly, in this study we not only demonstrated that DEX treatment increases cell stiffness, but also elevates the expression of proteins αSMA and phosphorylated-ERK1/2 associated with the contractility machinery of the TM; αSMA is a mechanosensitive protein whose overexpression can

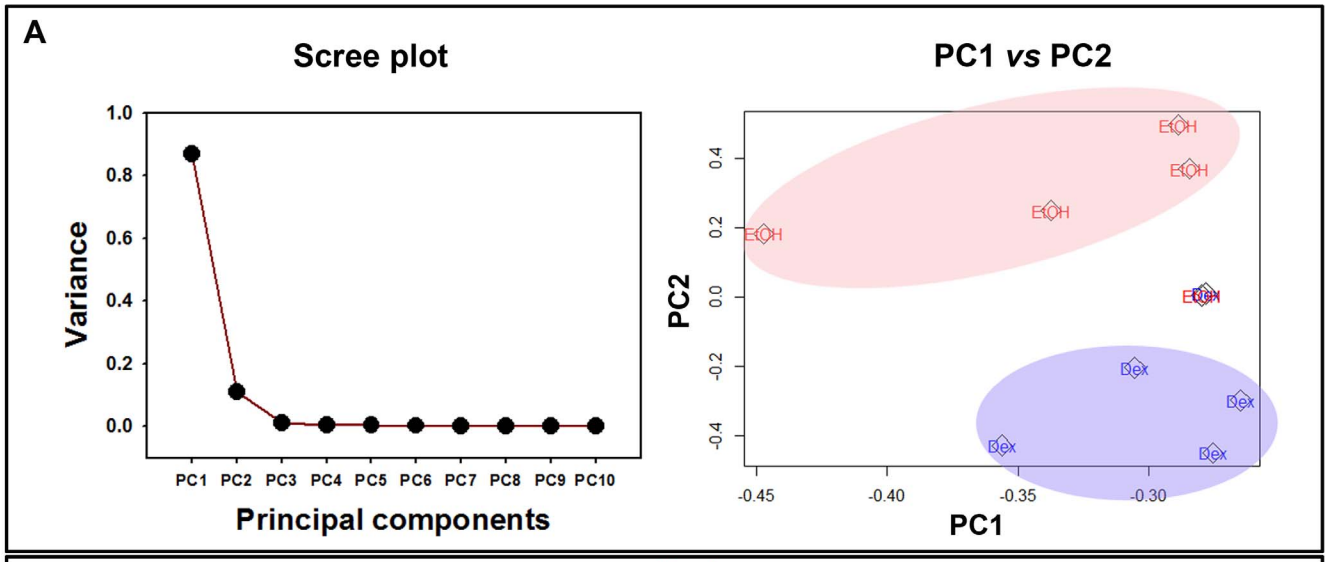

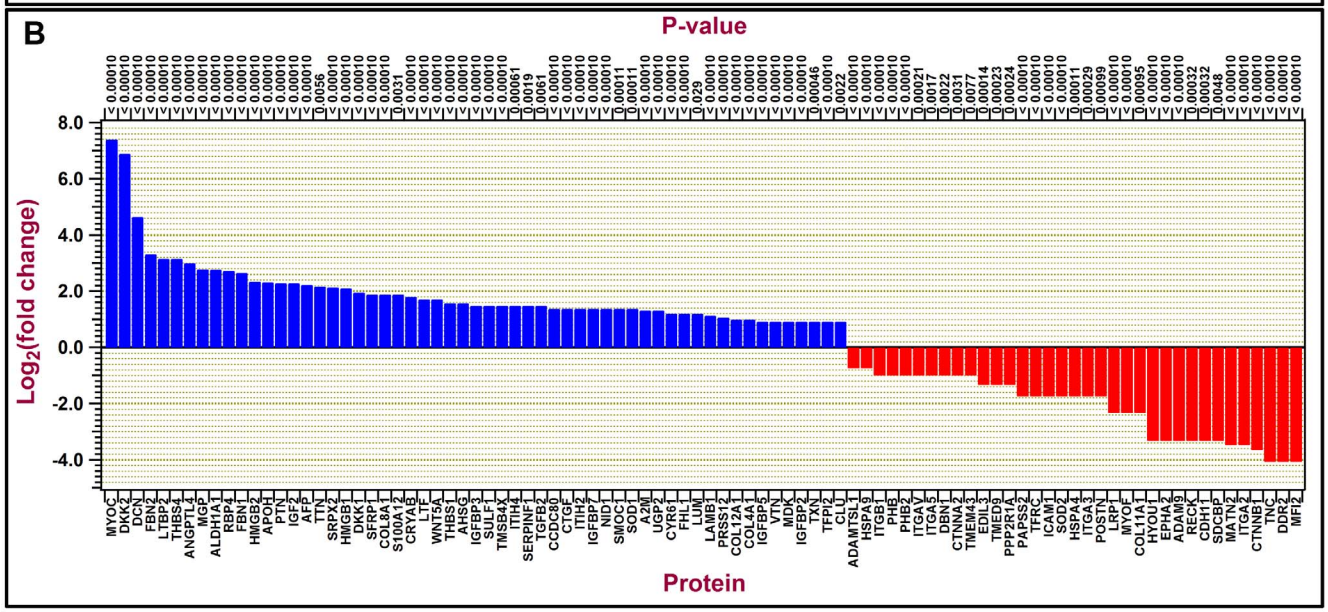

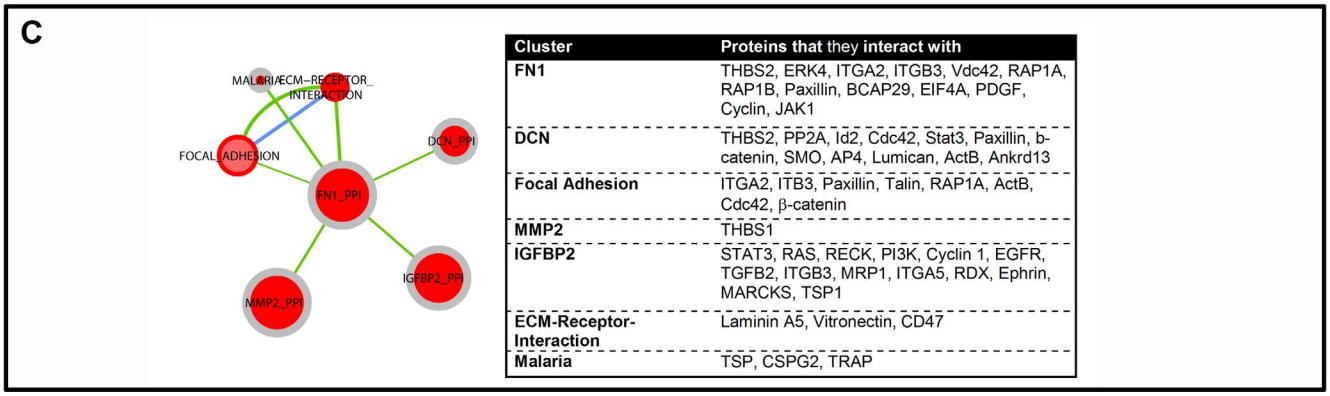

Cluster	Proteins that they interact with
FN1	THBS2, ERK4, ITGA2, ITGB3, Vdc42, RAP1A, RAP1B, Paxillin, BCAP29, EIF4A, PDGF, Cyclin, JAK1
DCN	THBS2, PP2A, Id2, Cdc42, Stat3, Paxillin, b-catenin, SMO, AP4, Lumican, ActB, Ankrd13
Focal Adhesion	ITGA2, ITB3, Paxillin, Talin, RAP1A, ActB, Cdc42, β-catenin
MMP2	THBS1
IGFBP2	STAT3, RAS, RECK, PI3K, Cyclin 1, EGFR, TGFB2, ITGB3, MRP1, ITGA5, RDX, Ephrin, MARCKS, TSP1
ECM-Receptor-Interaction	Laminin A5, Vitronectin, CD47
Malaria	TSP, CSPG2, TRAP

Figure 6. Quantitative analysis of mass spectral data of over 5100 proteins identified from cell-derived extracellular matrices after DEX and control treatments. Proteins were identified by X! Tandem LC-MS/MS. Matrices were derived from five donor lines. (**A**) Principal component analysis plots: scree plot identifying the number of principal components that define the proportion of variance in data is illustrated. Plot of PC1 versus PC2 demonstrates data clustering for 4 of 5 donor lines. (**B**) Histogram illustrating log to the base 2-fold changes of ECM protein expression comparing DEX with control cultures. Proteins that were upregulated are in *blue* and those downregulated are in *red* comparing DEX with control cultures. (**C**) Protein–protein interaction clusters of those most abundantly enriched identified by KEGG pathway analysis of ECM proteins. In the pathway graph, the center part of the *dot* represents the enrichment of upregulated proteins and the outer layer of the dot corresponds to the enrichment of the downregulated proteins. *Red center* at the nodes indicates that protein set is enriched in proteins that are upregulated, *gray* indicates proteins that are not enriched in downregulated group. *Green edge color* indicates that there are overlapped proteins (similarity) between the two nodes connecting the upregulated proteins. *Blue edge color* indicates that there are overlapped proteins between the two nodes connecting the downregulated proteins. If a node is *solid red*, which means that this protein set is enriched in up- and downregulated protein. The Table lists the proteins that each cluster interacts with.

Investigative Ophthalmology & Visual Science

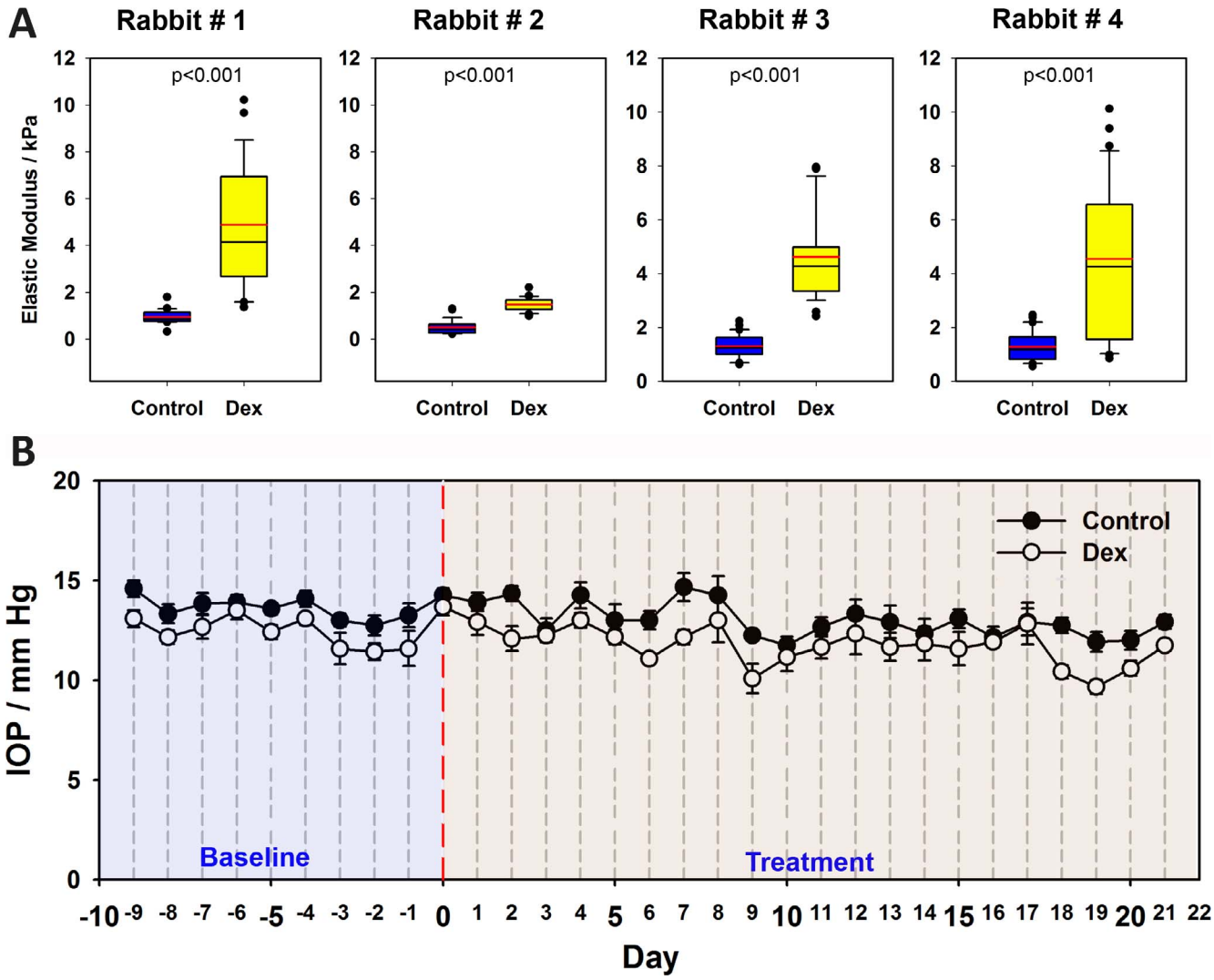

Figure 7. (**A**) Elastic modulus of trabecular meshwork from four rabbits treated with either vehicle control (left eye) or dexamethasone (DEX; right eye) after 21 days. Data are represented as *box plots* with mean indicated as a *red line*. Results are from at least seven locations with five force curves per location. $P < 0.001$, Mann-Whitney U test. (**B**) Changes in IOP of four rabbits recorded over 10 days before (baseline) and 21 days after treatment with vehicle control or DEX. Results are mean ± SD ($n = 4$ animals).

increase contractility[50,51] of cells by being incorporated into stress fibers.[52] Activation of the ERK pathway, an important constituent of the mitogen activated protein kinase (MAPK) family, points toward another potential clinical target for the regulation of stress fibers and mechanotransduction response. We recognize that, while cell stiffness does not equate to contractility, the presence of stress fibers provide the machinery for cells to exert contractile forces on the ECM.[53,54] Further, HTM cells presented significantly elevated numbers of stress fibers (F-actin) when treated over 4 weeks indicating that the biomechanical attributes of the cells are altered long-term. Future studies will determine if DEX treatment, indeed, modulates contractile forces exerted by HTM cells in vitro.

Treatment With DEX Alters the Biophysical Properties, Biochemical Composition, and Organization of ECM In Vitro

Using atomic force microscopy, a relevant method to study substrate rigidity on cellular length scales,[55,56] we demonstrated here that DEX-treated HTM cells deposit ECM that is significantly stiffer than those deposited by control cultures. Our results indicated that HTM cells, through deposition and modification of ECM, regulate their biophysical as well as biochemical environment. Concurrent with change in stiffness of the ECM, morphology, assembly, and expression of a number of ECM proteins were significantly altered. Even though expression of fibronectin (determined by proteomics) was similar, the architecture (determined by immunostaining) of the matrices elaborated by DEX- and vehicle-treated HTM cells was strikingly different. Fibronectin in DEX ECM was observed to be organized sheet-like, while in vehicle ECM it was diffuse. Glucocorticoid-induced fibronectin synthesis and assembly are reported to be partially dependent on the integrin receptor binding reflecting an inside-out signaling mechanism.[57–60] More recently, an in vitro study demonstrated that externally applied mechanical stress can transform the compact structure of fibronectin to its fibrillar state.[61] Thus, increased activation of contractility machinery and perhaps altered integrin binding in DEX-treated cells may contribute to the reorganization of deposited fibronectin.

In addition to these morphological changes, a significant number of proteins in the extracellular milieu were either up- or downregulated. Notably, MYOC, DCN, DKK2, fibrillin-1, fibrillin-2, thrombospondin 4 (THBS4), angiopoeitin-related protein 4 (ANGPTL4), and matrix-gla protein were upregulated 6-fold or more in the ECM after DEX treatment. Tellingly, we observed elevated expression of microfibril-associated proteins (fibrillin-1, fibrillin-2, LTBP2, ADAMTSL4) in the ECM derived from DEX-treated cells. Microfibrils are well established components of the ECM, in elastic and nonelastic tissues, and have been linked with the control and activation of TGF-β signaling.[62] Fibrillin-1 is a calcium binding glycoprotein (approximately 350 kDa) and a principal structural component of microfibrils of connective tissue ECM.[63] It has been postulated that fibrillar assembly of fibronectin (as observed in this study) is essential for the deposition and assembly of fibrillin-1[64] and that subsequent ECM microfibril formation is accelerated by extracellular ADAMTSL4.[65] Latent TGF binding protein-2 (LTBP2), whose mutations have been associated with primary congenital glaucoma,[66,67] is a component of mature ECM and depends on preformed fibrillin-1 network.[68] Defects in microfibrils, while most commonly studied with relevance to Marfan syndrome,[69] only recently have been hypothesized to have a role in glaucoma.[70] To the best of our knowledge, this is the first study to report increased expression of microfibril-associated proteins in the ECM of TM cells after chronic steroid treatment, although the presence of fibrillin-1 and microfibril-associated proteins have been documented previously in the JCT and corneoscleral meshwork of normal human eyes.[71,72]

Antagonists of the Wnt pathway DKK1,[73,74] SFRP1,[75,76] and Wnt5A[77] were overexpressed greater than 3-fold in the extracellular milieu of DEX-treated cells. The presence of Wnt antagonists in the stiffer ECM after steroid treatment revealed a link between cytoskeletal remodeling, glucocorticoid response, and ECM remodeling. Previous reports have documented that treatment of TM cells with SFRP1 elevates IOP and reduces outflow facility.[78,79] Prolonged inhibition of Wnt also has been linked to loss of cell–cell communication resulting in apoptosis, reduced cellularity, or senescence,[80–84] all of which have been hypothesized to have a role in progression of glaucoma.[85–87] We recently demonstrated that Wnt inhibition and senescence can alter cytoskeletal dynamics and increase cell stiffness.[88,89] Concomitant with this, cadherin-11 (CDH11), an integral membrane protein that promotes intercellular adhesion,[90] was found downregulated in the ECM after DEX treatment. While CDH11 has been postulated to have extracellular function in the formation of otholithic membranes,[91] their role in maintaining TM cellularity is unknown.

In addition, ECM proteins related to fibrosis also were overexpressed after chronic DEX treatment: thrombospondin 1,[92] TGF-β2,[93–95] lumican,[96] and CTGF or CCN2.[97–100] Two members of the CCN family proteins (CCN1 [CYR61] and CCN2 [CTG]), upregulated after steroid treatment, can be activated and secreted when cells are mechanically challenged.[101] We noted that thymosin β4, another protein upregulated with DEX treatment, has been linked previously to reorganizing connective tissue during wound repair[102] and is a potent regulator of actin polymerization.[103] In aggregate, these proteomic findings suggest profound alterations of ECM mechanobiology in DEX-treated TM cells.

DEX Treatment Stiffens the TM In Vivo

Using the rabbit model, we demonstrated that, although no changes in IOP were observed between the DEX-treated and control eyes over the duration of the study in our older rabbits, the TMs in DEX-treated eyes were significantly stiffer than controls in just 3 weeks. To our knowledge, this is the first study to demonstrate in vivo that the mechanical properties of the meshwork tissue are altered after topical treatment with steroids irrespective of any measured change in IOP. What the consequences of prolonged application of steroids in these older animals would be on IOP changes and subsequent tissue biomechanics is speculative at this point and warrants further investigation. Studies correlating ultrastructural changes of the TM in rabbits with altered mechanical properties after steroid treatment are further needed. Glucocorticoid-induced modifications to the TM, with unknown biomechanical consequences to the TM, after systemic delivery of DEX have been reported in mice recently.[104] Whether altered biomechanics contributes to IOP changes in the long term in rabbits remains to be elucidated. Further studies will be required to elaborate the role of GCs in altering TM biomechanics in younger rabbits with steroid-induced ocular hypertension.

Summary

Data presented here definitively demonstrate that biophysical and biochemical dynamics of cells and ECM, in vitro and in vivo, are directly altered when treated with DEX. Importantly, we demonstrated that biomechanical attributes of the TM in vivo are significantly altered regardless of changes in IOP. In vitro, acute treatment of HTM cells with DEX makes them stiffer and possibly more contractile. Increased tension between cell and substratum via focal adhesions can trigger transcriptional changes in the long term resulting in altered deposition and assembly of ECM. Indeed, DEX treatment resulted in a stiffer yet more organized matrix that was rich in Wnt inhibitors, proteins associated as fibrotic markers, and inhibitors of matrix degradation. These can in turn result in a sustained feedback loop that may lead to further stiffening of the cytoskeleton and subsequently matrix, therefore, contributing to the pathophysiology of steroid-induced ocular hypertension.

Online Supplemental Material

Details of experimental procedures related to contact mechanics and shotgun proteomics can be found in supplementary methods. Raw data of proteomics with total spectral counts are available as "Data S1.xls." The KEGG analyses and visualization of GO enrichment are illustrated in Supplementary Figures.

Acknowledgments

The authors thank Yow-Ren Chang, BS, Linda Huang, Monica Motta, BS, RVT, Geneva Tripp, BS, and Allison Calderon for technical assistance, and Jie Li, PhD, and Blythe Durbin-Johnson, PhD, for help with the KEGG analysis.

Supported by NIH Grants R01EY019475, P30EY12576, and unrestricted funds from Research to Prevent Blindness. The authors alone are responsible for the content and writing of the paper.

Disclosure: **V.K. Raghunathan**, None; **J.T. Morgan**, None; **S.A. Park**, None; **D. Weber**, None; **B.S. Phinney**, None; **C.J. Murphy**, None; **P. Russell**, None

References

1. Quigley HA, Broman AT. The number of people with glaucoma worldwide in 2010 and 2020. *Br J Ophthalmol*. 2006;90:262–267.
2. Last JA, Pan T, Ding Y, et al. Elastic modulus determination of normal and glaucomatous human trabecular meshwork. *Invest Ophthalmol Vis Sci*. 2011;52:2147–2152.

3. Clark AF. The cell and molecular biology of glaucoma: biomechanical factors in glaucoma. *Invest Ophthalmol Vis Sci*. 2012;53:2473–2475.
4. Clark AF, Wilson K, McCartney MD, Miggans ST, Kunkle M, Howe W. Glucocorticoid-induced formation of cross-linked actin networks in cultured human trabecular meshwork cells. *Invest Ophthalmol Vis Sci*. 1994;35:281–294.
5. Rohen JW, Lütjen-Drecoll E, Flügel C, Meyer M, Grierson I. Ultrastructure of the trabecular meshwork in untreated cases of primary open-angle glaucoma (POAG). *Exp Eye Res*. 1993; 56:683–692.
6. Filla MS, Clark R, Peters DM. A syndecan-4 binding peptide derived from laminin 5 uses a novel PKCε pathway to induce cross-linked actin network (CLAN) formation in human trabecular meshwork (HTM) cells. *Exp Cell Res*. 2014;327: 171–182.
7. Filla MS, Woods A, Kaufman PL, Peters DM. β1 and β3 integrins cooperate to induce syndecan-4-containing cross-linked actin networks in human trabecular meshwork cells. *Invest Ophthalmol Vis Sci*. 2006;47:1956–1967.
8. Tovar-Vidales T, Roque R, Clark AF, Wordinger RJ. Tissue transglutaminase expression and activity in normal and glaucomatous human trabecular meshwork cells and tissues. *Invest Ophthalmol Vis Sci*. 2008;49:622–628.
9. Xue W, Comes N, Borrás T. Presence of an established calcification marker in trabecular meshwork tissue of glaucoma donors. *Invest Ophthalmol Vis Sci*. 2007;48:3184–3194.
10. Yip CYY, Chen J-H, Zhao R, Simmons CA. Calcification by Valve Interstitial Cells Is Regulated by the Stiffness of the Extracellular Matrix. *Atertio Thromb Vasc Biol*. 2009;29: 936–942.
11. Santhanam L, Tuday EC, Webb AK, et al. Decreased S-nitrosylation of tissue transglutaminase contributes to age-related increases in vascular stiffness. *Circ Res*. 2010;107: 117–125.
12. Jung SM, Jandu S, Steppan J, et al. Increased tissue transglutaminase activity contributes to central vascular stiffness in eNOS knockout mice. *Am J Physiol Heart Circ Physiol*. 2013;305:H803–H810.
13. Raghunathan VK, Morgan JT, Dreier B, et al. Role of substratum stiffness in modulating genes associated with extracellular matrix and mechanotransducers YAP and TAZ. *Invest Ophthalmol Vis Sci*. 2013;54:378–386.
14. Schlunck G, Han H, Wecker T, Kampik D, Meyer-ter-Vehn T, Grehn F. Substrate rigidity modulates cell–matrix interactions and protein expression in human trabecular meshwork cells. *Invest Ophthalmol Vis Sci*. 2008;49:262–269.
15. Thomasy SM, Morgan JT, Wood JA, Murphy CJ, Russell P. Substratum stiffness and latrunculin B modulate the gene expression of the mechanotransducers YAP and TAZ in human trabecular meshwork cells. *Exp Eye Res*. 2013;113: 66–73.
16. Thomasy SM, Wood JA, Kass PH, Murphy CJ, Russell P. Substratum stiffness and latrunculin B regulate matrix gene and protein expression in human trabecular meshwork cells. *Invest Ophthalmol Vis Sci*. 2012;53:952–958.
17. Wood JA, McKee CT, Thomasy SM, et al. Substratum compliance regulates human trabecular meshwork cell behaviors and response to latrunculin B. *Invest Ophthalmol Vis Sci*. 2011;52:9298–9303.
18. Gasiorowski JZ, Russell P. Biological properties of trabecular meshwork cells. *Exp Eye Res*. 2009;88:671–675.
19. Polansky JR, Fauss DJ, Zimmerman CC. Regulation of TIGR/MYOC gene expression in human trabecular meshwork cells. *Eye*. 2000;14:503–514.
20. Schwartz B, McCarty G, Rosner B. Increased plasma free cortisol in ocular hypertension and open angle glaucoma. *Arch Ophthalmol*. 1987;105:1060–1065.
21. Schwartz B, Rabin PA, Wysocki A, Martin J. Decreased plasma cortisol in response to intramuscular ACTH in ocular hypertensives and primary open-angle glaucomas. *J Glaucoma*. 2007;16:282–286.
22. Schwartz B, Wysocki A, Qi Y. Decreased response of plasma cortisol to intravenous metyrapone in ocular hypertension and primary open-angle glaucoma. *J Glaucoma*. 2005;14: 474–481.
23. Stokes J, Walker BR, Campbell JC, Seckl JR, O'Brien C, Andrew R. Altered peripheral sensitivity to glucocorticoids in primary open-angle glaucoma. *Invest Ophthalmol Vis Sci*. 2003;44:5163–5167.
24. Weinstein B, Munnangi P, Gordon G, Southren A. Defects in cortisol-metabolizing enzymes in primary open-angle glaucoma. *Invest Ophthalmol Vis Sci*. 1985;26:890–893.
25. Clark AF, Morrison JC. Steroid-induced glaucoma. In: Morrison JC, Pollack IP, eds. *Glaucoma: Science and Practice*. New York, NY: Thieme Medical Publishers, Inc.; 2002:197–206.
26. Kitazawa Y, Horie T. The prognosis of corticosteroid-responsive individuals. *Arch Ophthalmol*. 1981;99:819–823.
27. Lewis JM, Priddy T, Judd J, et al. Intraocular pressure response to topical dexamethasone as a predictor for the development of primary open-angle glaucoma. *Am J Ophthalmol*. 1988;106:607–612.
28. Bollinger KE, Crabb JS, Yuan X, Putliwala T, Clark AF, Crabb JW. Proteomic similarities in steroid responsiveness in normal and glaucomatous trabecular meshwork cells. *Mol Vis*. 2012; 18:2001–2011.
29. Clark AF, Steely HT, Dickerson JE Jr, et al. Glucocorticoid induction of the glaucoma gene MYOC in human and monkey trabecular meshwork cells and tissues. *Invest Ophthalmol Vis Sci*. 2001;42:1769–1780.
30. Steely HT, Browder SL, Julian MB, Miggans ST, Wilson KL, Clark AF. The effects of dexamethasone on fibronectin expression in cultured human trabecular meshwork cells. *Invest Ophthalmol Vis Sci*. 1992;33:2242–2250.
31. Zhou L, Li Y, Yue BY. Glucocorticoid effects on extracellular matrix proteins and integrins in bovine trabecular meshwork cells in relation to glaucoma. *Int J Mol Med*. 1998;1:339–346.
32. Morgan JT, Wood JA, Walker NJ, et al. Human trabecular meshwork cells exhibit several characteristics of, but are distinct from, adipose-derived mesenchymal stem cells. *J Ocul Pharmacol Ther*. 2014;30:254–266.
33. National Institute of Health. ImageJ. Image processing and analysis in Java. Available at: http://imagej.nih.gov/ij/. Accessed February 2010.
34. Schneider CA, Rasband WS, Eliceiri KW. NIH Image to ImageJ: 25 years of image analysis. *Nat Methods*. 2012;9:671–675.
35. Raghunathan VK, Morgan JT, Chang Y-R, et al. Transforming growth factor beta 3 modifies mechanics and composition of extracellular matrix deposited by human trabecular meshwork cells. *ACS Biomat Sci Eng*. 2015;1:110–118.
36. Huang DW, Sherman BT, Lempicki RA. Systematic and integrative analysis of large gene lists using DAVID bioinformatics resources. *Nat Protocols*. 2008;4:44–57.
37. Morgan JT, Raghunathan VK, Thomasy SM, Murphy CJ, Russell P. Robust and artifact-free mounting of tissue samples for atomic force microscopy. *BioTechniques*. 2014;56:40–42.
38. McKee CT, Raghunathan VK, Nealey PF, Russell P, Murphy CJ. Topographic modulation of the orientation and shape of cell nuclei and their influence on the measured elastic modulus of epithelial cells. *Biophys J*. 2011;101:2139–2146.
39. McKee CT, Wood JA, Shah NM, et al. The effect of biophysical attributes of the ocular trabecular meshwork associated with glaucoma on the cell response to therapeutic agents. *Biomaterials*. 2011;32:2417–2423.

Investigative Ophthalmology & Visual Science

40. Zhang B, VerBerkmoes NC, Langston MA, Uberbacher E, Hettich RL, Samatova NF. Detecting differential and correlated protein expression in label-free shotgun proteomics. *J Proteome Res*. 2006;5:2909–2918.
41. Knepper PA, Breen M, Weinstein HG, Blacik LJ. Intraocular pressure and glycosaminoglycan distribution in the rabbit eye: effect of age and dexamethasone. *Exp Eye Res*. 1978;27:567–575.
42. Qin Y, Lam S, Yam GH, et al. A rabbit model of age-dependent ocular hypertensive response to topical corticosteroids. *Acta Ophthalmol*. 2012;90:559–563.
43. Johnson D, Gottanka J, Flugel C, Hoffmann F, Futa R, Lutjen-Drecoll E. Ultrastructural changes in the trabecular meshwork of human eyes treated with corticosteroids. *Arch Ophthalmol*. 1997;115:375–383.
44. Clark AF, Wilson K, de Kater AW, Allingham RR, McCartney MD. Dexamethasone-induced ocular hypertension in perfusion-cultured human eyes. *Invest Ophthalmol Vis Sci*. 1995;36:478–489.
45. Clark AF, Brotchie D, Read AT, et al. Dexamethasone alters F-actin architecture and promotes cross-linked actin network formation in human trabecular meshwork tissue. *Cell Motil Cytoskeleton*. 2005;60:83–95.
46. Clark R, Nosie A, Walker T, et al. Comparative genomic and proteomic analysis of cytoskeletal changes in dexamethasone-treated trabecular meshwork cells. *Mol Cell Proteomics*. 2013;12:194–206.
47. Yuan Y, Call MK, Yuan Y, et al. Dexamethasone induces cross-linked actin networks in trabecular meshwork cells through noncanonical wnt signaling. *Invest Ophthalmol Vis Sci*. 2013;54:6502–6509.
48. Rao V, Epstein D. Rho GTPase/Rho kinase inhibition as a novel target for the treatment of glaucoma. *Biodrugs*. 2007;21:167–177.
49. Wang SK, Chang RT. An emerging treatment option for glaucoma: rho kinase inhibitors. *Clin Ophthalmol*. 2014;8:883–890.
50. Hinz B, Celetta G, Tomasek JJ, Gabbiani G, Chaponnier C. Alpha-smooth muscle actin expression upregulates fibroblast contractile activity. *Mol Biol Cell*. 2001;12:2730–2741.
51. Chen J, Li H, SundarRaj N, Wang JHC. Alpha-smooth muscle actin expression enhances cell traction force. *Cell Motil Cytoskeleton*. 2007;64:248–257.
52. Skalli O, Gabbiani F, Gabbiani G. Action of general and alpha-smooth muscle-specific actin antibody microinjection on stress fibers of cultured smooth muscle cells. *Exp Cell Res*. 1990;187:119–125.
53. Kumar S, Maxwell IZ, Heisterkamp A, et al. Viscoelastic retraction of single living stress fibers and its impact on cell shape, cytoskeletal organization, and extracellular matrix mechanics. *Biophys J*. 2006;90:3762–3773.
54. Chrzanowska-Wodnicka M, Burridge K. Rho-stimulated contractility drives the formation of stress fibers and focal adhesions. *J Cell Biol*. 1996;133:1403–1415.
55. Engler AJ, Richert L, Wong JY, Picart C, Discher DE. Surface probe measurements of the elasticity of sectioned tissue, thin gels and polyelectrolyte multilayer films: correlations between substrate stiffness and cell adhesion. *Surf Sci*. 2004;570:142–154.
56. Last JA, Russell P, Nealey PF, Murphy CJ. The applications of atomic force microscopy to vision science. *Invest Ophthalmol Vis Sci*. 2010;51:6083–6094.
57. McKeown-Longo PJ, Mosher DF. Interaction of the 70,000-mol-wt amino-terminal fragment of fibronectin with the matrix-assembly receptor of fibroblasts. *J Cell Biol*. 1985;100:364–374.
58. Oliver N, Newby RF, Furcht LT, Bourgeois S. Regulation of fibronectin biosynthesis by glucocorticoids in human fibrosarcoma cells and normal fibroblasts. *Cell*. 1983;33:287–296.
59. Brenner KA, Corbett SA, Schwarzbauer JE. Regulation of fibronectin matrix assembly by activated Ras in transformed cells. *Oncogene*. 2000;19:3156–3163.
60. Fogerty FJ, Mosher DF. Mechanisms for organization of fibronectin matrix. *Cell Differ Dev*. 1990;32:439–450.
61. Nguyen HTT, Huynh KC, Scharf RE, Stoldt VR. Shear-related fibrillogenesis of fibronectin. *Biol Chem*. 2013;394:1495–1503.
62. Ramirez F, Rifkin DB. Extracellular microfibrils: contextual platforms for TGFbeta and BMP signaling. *Curr Opin Cell Biol*. 2009;21:616–622.
63. Handford PA. Fibrillin-1, a calcium binding protein of extracellular matrix. *Biochim Biophys Acta*. 2000;1498:84–90.
64. Kinsey R, Williamson MR, Chaudhry S, et al. Fibrillin-1 microfibril deposition is dependent on fibronectin assembly. *J Cell Sci*. 2008;121:2696–2704.
65. Gabriel LAR, Wang LW, Bader H, et al. ADAMTSL4, a secreted glycoprotein widely distributed in the eye, binds fibrillin-1 microfibrils and accelerates microfibril biogenesis. *Invest Ophthalmol Vis Sci*. 2012;53:461–469.
66. Ali M, McKibbin M, Booth A, et al. Null mutations in LTBP2 cause primary congenital glaucoma. *Am J Hum Genet*. 2009;84:664–671.
67. Jelodari-Mamaghani S, Haji-Seyed-Javadi R, Suri F, et al. Contribution of the latent transforming growth factor-β binding protein 2 gene to etiology of primary open angle glaucoma and pseudoexfoliation syndrome. *Mol Vis*. 2013;19:333–347.
68. Massam-Wu T, Chiu M, Choudhury R, et al. Assembly of fibrillin microfibrils governs extracellular deposition of latent TGF beta. *J Cell Sci*. 2010;123:3006–3018.
69. Hubmacher D, Apte SS. The biology of the extracellular matrix: novel insights. *Curr Opin Rheumatol*. 2013;25:65–70.
70. Kuchtey J, Kuchtey RW. The microfibril hypothesis of glaucoma: implications for treatment of elevated intraocular pressure. *J Ocul Pharmacol Ther*. 2014;30:170–180.
71. Ueda J, Wentz-Hunter K, Yue BY. Distribution of myocilin and extracellular matrix components in the juxtacanalicular tissue of human eyes. *Invest Ophthalmol Vis Sci*. 2002;43:1068–1076.
72. Ueda J, Yue BY. Distribution of myocilin and extracellular matrix components in the corneoscleral meshwork of human eyes. *Invest Ophthalmol Vis Sci*. 2003;44:4772–4779.
73. Fedi P, Bafico A, Nieto Soria A, et al. Isolation and biochemical characterization of the human Dkk-1 homologue, a novel inhibitor of mammalian Wnt signaling. *J Biol Chem*. 1999;274:19465–19472.
74. Glinka A, Wu W, Delius H, Monaghan AP, Blumenstock C, Niehrs C. Dickkopf-1 is a member of a new family of secreted proteins and functions in head induction. *Nature*. 1998;391:357–362.
75. He J, Sheng T, Stelter AA, et al. Suppressing Wnt signaling by the Hedgehog Pathway through sFRP-1. *J Biol Chem*. 2006;281:35598–35602.
76. Bhat RA, Stauffer B, Komm BS, Bodine PVN. Structure–function analysis of secreted frizzled-related protein-1 for its Wnt antagonist function. *J Cell Biochem*. 2007;102:1519–1528.
77. Topol L, Jiang X, Choi H, Garrett-Beal L, Carolan PJ, Yang Y. Wnt-5a inhibits the canonical Wnt pathway by promoting GSK-3-independent beta-catenin degradation. *J Cell Biol*. 2003;162:899–908.
78. Wang WH, McNatt LG, Pang IH, et al. Increased expression of the WNT antagonist sFRP-1 in glaucoma elevates intraocular pressure. *J Clin Invest*. 2008;118:1056–1064.

Investigative Ophthalmology & Visual Science

79. Mao W, Millar JC, Wang W-H, et al. Existence of the canonical Wnt signaling pathway in the human trabecular meshwork. *Invest Ophthalmol Vis Sci*. 2012;53:7043–7051.
80. Gess B, Halfter H, Kleffner I, et al. Inhibition of N-cadherin and β-catenin function reduces axon-induced Schwann cell proliferation. *J Neurosci Res*. 2008;86:797–812.
81. Verma UN, Surabhi RM, Schmaltieg A, Becerra C, Gaynor RB. Small interfering RNAs directed against β-catenin inhibit the in vitro and in vivo growth of colon cancer cells. *Clin Cancer Res*. 2003;9:1291–1300.
82. Bodine PVN, Billiard J, Moran RA, et al. The Wnt antagonist secreted frizzled-related protein-1 controls osteoblast and osteocyte apoptosis. *J Cell Biochem*. 2005;96:1212–1230.
83. Zhang K-S, Zhou Q, Wang Y-F, Liang L-J. Inhibition of Wnt signaling induces cell apoptosis and suppresses cell proliferation in cholangiocarcinoma cells. *Oncol Rep*. 2013;30:1430–1438.
84. Elzi DJ, Song M, Hakala K, Weintraub ST, Shiio Y. Wnt antagonist SFRP1 functions as a secreted mediator of senescence. *Mol Cell Biol*. 2012;32:4388–4399.
85. Alvarado J, Murphy C, Juster R. Trabecular meshwork cellularity in primary open-angle glaucoma and nonglaucomatous normals. *Ophthalmology*. 1984;91:564.
86. Baleriola J, Garcia-Feijoo J, Martinez-de-la-Casa JM, Fernandez-Cruz A, de la Rosa EJ, Fernandez-Durango R. Apoptosis in the trabecular meshwork of glaucomatous patients. *Mol Vis*. 2008;14:1513–1516.
87. Liton PB, Challa P, Stinnett S, Luna C, Epstein DL, Gonzalez P. Cellular senescence in the glaucomatous outflow pathway. *Exp Gerontol*. 2005;40:745–748.
88. Morgan JT, Raghunathan VK, Chang YR, Murphy CJ, Russell P. Wnt inhibition induces persistent increases in intrinsic stiffness of human trabecular meshwork cells. *Exp Eye Res*. 2015;132C:174–178.
89. Morgan JT, Raghunathan VK, Chang Y-R, Murphy CJ, Russell P. The intrinsic stiffness of human trabecular meshwork cells increases with senescence [published online ahead of print April 12, 2015]. *Oncotarget*.
90. Valencia X, Higgins JM, Kiener HP, et al. Cadherin-11 provides specific cellular adhesion between fibroblast-like synoviocytes. *J Exp Med*. 2004;200:1673–1679.
91. Clendenon SG, Shah B, Miller CA, et al. Cadherin-11 controls otolith assembly: evidence for extracellular cadherin activity. *Dev Dyn*. 2009;238:1909–1922.
92. Flügel-Koch C, Ohlmann A, Fuchshofer R, Welge-Lüssen U, Tamm ER. Thrombospondin-1 in the trabecular meshwork: localization in normal and glaucomatous eyes, and induction by TGF-[beta] 1 and dexamethasone in vitro. *Exp Eye Res*. 2004;79:649–663.
93. Fuchshofer R, Welge-Lussen U, Lütjen-Drecoll E. The effect of TGF-β2 on human trabecular meshwork extracellular proteolytic system. *Exp Eye Res*. 2003;77:757–765.
94. Sethi A, Jain A, Zode GS, Wordinger RJ, Clark AF. Role of TGFbeta/Smad signaling in gremlin induction of human trabecular meshwork extracellular matrix proteins. *Invest Ophthalmol Vis Sci*. 2011;52:5251–5259.
95. Fitzgerald AM, Benz C, Clark AF, Wordinger RJ. The effects of transforming growth factor-?2 on the expression of follistatin and activin a in normal and glaucomatous human trabecular meshwork cells and tissues. *Invest Ophthalmol Vis Sci*. 2012;53:7358–7369.
96. Krishnan A, Li X, Kao WWY, et al. Lumican, an extracellular matrix proteoglycan, is a novel requisite for hepatic fibrosis. *Lab Invest*. 2012;92.
97. Leask A, Parapuram SK, Shi-wen X, Abraham D. Connective tissue growth factor (CTGF, CCN2) gene regulation: a potent clinical bio-marker of fibroproliferative disease? *J Cell Commun Signal*. 2009;3:89–94.
98. Shi-wen X, Pennington D, Holmes A, et al. Autocrine overexpression of CTGF maintains fibrosis: RDA analysis of fibrosis genes in systemic sclerosis. *Exp Cell Res*. 2000;259:213–224.
99. Browne JG, Ho SL, Kane R, et al. Connective tissue growth factor is increased in pseudoexfoliation glaucoma. *Invest Ophthalmol Vis Sci*. 2011;52:3660–3666.
100. Chudgar SM, Deng P, Maddala R, Epstein DL, Rao PV. Regulation of connective tissue growth factor expression in the aqueous humor outflow pathway. *Mol Vis*. 2006;12:1117–1126.
101. Chaqour B, Goppelt-Struebe M. Mechanical regulation of the Cyr61/CCN1 and CTGF/CCN2 proteins. *FEBS J*. 2006;273:3639–3649.
102. Ehrlich HP, Hazard SW III. Thymosin β4 enhances repair by organizing connective tissue and preventing the appearance of myofibroblasts. *Ann N Y Acad Sci*. 2010;1194:118–124.
103. Sanders MC, Goldstein AL, Wang YL. Thymosin beta 4 (Fx peptide) is a potent regulator of actin polymerization in living cells. *Proc Natl Acad Sci U S A*. 1992;89:4678–4682.
104. Overby DR, Bertrand J, Tektas O-Y, et al. Ultrastructural changes associated with dexamethasone-induced ocular hypertension in mice. *Invest Ophthalmol Vis Sci*. 2014;55:4922–4933.

Investigative Ophthalmology & Visual Science